Earth and Planetary Science Letters 539 (2020) 116214

Contents lists available at ScienceDirect

Earth and Planetary Science Letters

www.elsevier.com/locate/epsl

Upper mantle tomography beneath the Pacific Northwest interior

A. Christian Stanciu *, Eugene D. Humphreys

Department of Earth Sciences, University of Oregon, 1272 University of Oregon, Eugene, OR, 97403, USA

ARTICLE INFO

Article history:
Received 22 October 2019
Received in revised form 25 February 2020
Accepted 8 March 2020
Available online xxxx
Editor: M. Ishii

Keywords:
seismic tomography
ray tracing
ray weighting
Pacific Northwest
Farallon
Wallowa

ABSTRACT

The Pacific Northwest has undergone extensive tectonic and magmatic construction in the Cenozoic, and many clues to its history are in a well-resolved upper mantle structure. We present new P, S, and V_P/V_S models that benefit from improved algorithms and additional data from recently deployed flexible array experiments in the region of the Columbia River Basalts, western Snake River Plain, and Idaho Batholith. We refine the geometries of previously imaged structures and identify new anomalies beneath the Pacific Northwest. A clear separation is resolved between the Wallowa and Idaho structures that extends from the base of the crust to the depth extent of these structures. The separation follows the Precambrian margin of North America, possibly indicating separate tectonic histories for the two structures. A shallow fast anomaly beneath Idaho Batholith may be responsible for the observed curvature of the Yellowstone track around this batholith. And a strong and unusually deep (180–250 km) slow anomaly is present east of the apparent Juan de Fuca slab gap. Resolving these structures well is important in understanding the origin of the lithospheric fragments in the mantle, and key to any reconstruction of the evolution of the Pacific Northwest-Farallon-Kula-Juan de Fuca tectonic system. Of most relevance, understanding the origin of the imaged high-velocity mantle structures provides strong constraint on their density, that otherwise would be largely unknown, which controls the evolution of vertical and horizontal stresses acting at the base of the lithosphere and hence the evolution of topography. Also, resolving the volumes of partially molten upper mantle shapes our understanding on the origin of the abundant volcanism in the Pacific Northwest interior.

1. Introduction

By providing high-quality continent-wide and lithosphere-deep continental resolution, and by enabling development of new imaging techniques, deployment of the Transportable Array of EarthScope's USArray led to important theoretical and observational seismic improvements. Unexpected and surprising structures have been imaged nearly everywhere beneath the U.S., illustrating that much about active and inactive continent is not well understood. The Pacific NW is especially rich with upper mantle structures, reflecting the especially active tectonic and magmatic evolution of the region.

Along the Cordilleran orogeny, the Pacific NW occupies a fundamental position of transition between continent defined by Mesozoic arc terrane accretion to the north and non-accretionary subduction to the south. During the course of the Cenozoic, Pacific NW lithosphere experienced regional construction with the accretion of the Siletzia ocean plateau, major magmatic modification with the initiation of the ignimbrite flareup, eruption of the Columbia River flood basalts and initiation of Cascade arc magmatism, and tectonic disruption with core-complex and Basin and Range extension and a rotation of several tens of degrees over most of the area.

Pacific Northwest upper mantle structure is largely a product of Cenozoic activity. However, pre-existing structures play an important role in controlling magmatism and deformation. Geochemical and isotopic evidence for 98–53 Ma Idaho Batholith emplacement indicate an increasing dominance of a crustal source and diminishing mantle contributions (Fig. 1, Gaschnig et al., 2011). During this time, Sevier and Laramide thrusting thickened the crust in the volcanic arc (e.g., Livaccari, 1991). Across the western U.S., the Laramide orogeny is characterized by arcs turning off and strong thrusting in the Rocky Mountains crust (e.g., Hamilton, 1989). These features have been attributed to slab flattening, although in the Pacific Northwest the possible presence of the Kula-Farallon spreading center may complicate our understanding of the Laramide orogeny there. At ~53 Ma, the Siletzia large igneous province accreted to North America (Duncan, 1982; Wells et al., 2014), followed immediately by the large Challis magmatic event in Idaho, 53–45 Ma (Fig. 1, Foster et al., 2001). This is thought to

* Corresponding author.
E-mail address: cstanciu@uoregon.edu (A.C. Stanciu).

https://doi.org/10.1016/j.epsl.2020.116214
0012-821X/

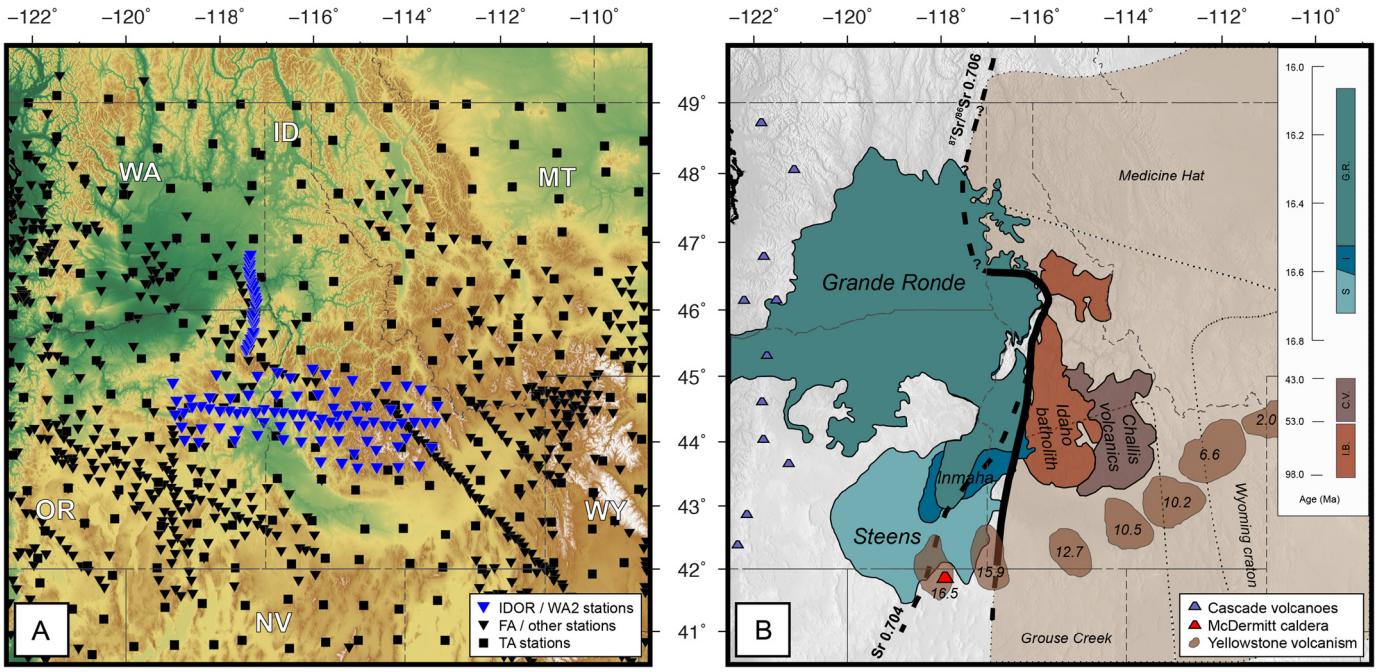

Fig. 1. (A) Region included in this study, showing seismic stations used (Wallowa2 and IDOR experiments - inverted blue triangles; US_TA array - black squares; flexible arrays and other deployments - inverted black triangles). (B) Map showing the major magmatic events in the last 100 Ma (after Reidel et al., 2013; Mueller et al., 2011; Gaschnig et al., 2011). Blue triangles show the location of the Cascade volcanoes. The brown shaded irregular patches show the age progressive calderas of Yellowstone silicic volcanism, with ages in m.y. (after Smith et al., 2009). Red triangle marks the location of McDermitt caldera. Thick continuous and dashed black lines mark the known and inferred location, respectively, of the $^{87}Sr/^{86}Sr$ 0.706 and 0.704 isopleths. Tan shaded area corresponds to Precambrian North America. Inset shows the time progression of the main eruptive phases of Idaho magmatism (Gashnig et al., 2011) and the CRBs (after Kasbohm and Schoene, 2018). (For interpretation of the colors in the figure(s), the reader is referred to the web version of this article.)

represent foundering of the flat Farallon slab from beneath western Montana and Idaho, creating the high-velocity Idaho curtain anomaly (Schmandt and Humphreys, 2011).

After a period of volcanic quiescence, Columbia River Basalt (CRB) volcanism erupted from eastern Oregon and nearby areas (Fig. 1) through crust immediately west of Precambrian North America (as represented by the $^{87}Sr/^{86}Sr$ 0.706 isopleth, Armstrong et al., 1977; Manduca et al., 1993), where Cenozoic magmatism had not occurred. This volcanism initiated at ∼16.7 Ma (Jarboe et al., 2010; Kasbohm and Schoene, 2018) from vents in SE Oregon and northern Nevada, approximately where and when it would be expected by back-projecting the Yellowstone hotspot track (Fig. 1). CRB volcanism is commonly thought to represent arrival of the Yellowstone plume to North America (e.g., Brandon and Goles, 1988; Camp and Hanan, 2008). Because there is good evidence that this hotspot created the Siletzia large igneous province before being overrun by North America ∼55 Ma (Duncan, 1982; Wells et al., 2014), CRB magmatism probably is not due to the arrival of a plume head created in the lower mantle. In the view of an already-active Yellowstone plume, the initiation and rather large size of the CRB involved arrival to North America of the large volume of plume mantle that accumulated beneath the subducting Farallon slab (Geist and Richards, 1993). Hales et al. (2005) suggested that delamination drove asthenospheric ascent and topographic uplift, and Darold and Humphreys (2013) argue that this ascent was important in amplifying plume-related volcanism.

CRB volcanism is characterized by a northward progression of geochemically distinct large volume flows (Camp and Ross, 2004; Wolff and Ramos, 2013, Fig. 1). The first to erupt were the Steens basalts in SE Oregon. From here volcanism migrated quickly northward, erupting the Imnaha and then the Grande Ronde flows before waning as magmatism reached the west-trending part of the suture with Precambrian crust in southern Washington (Fig. 1). The Grande Ronde lavas, comprising nearly three fourths of the total flood basalt volume (Reidel et al., 2013), represent a rapid expansion of volcanic activity 100s of kilometers north of the site of initial volcanism. These lavas contain a plume component similar to Imnaha, but unlike the earlier lavas, Grande Ronde lavas have an unusually high silica concentration. This indicates to most workers that this magma assimilated a large amount of continental crust (e.g., Wolff and Ramos, 2013). Furthermore, the lead isotopic signature indicates that these lavas are contaminated with cratonic crust similar to that of the Idaho Batholith (Wolff and Ramos, 2013), suggesting the Grande Ronde magma system extended east of the Precambrian suture.

Our paper reexamines upper mantle seismic structure beneath the Pacific NW interior using a recently enlarged dataset and technically upgraded teleseismic tomography algorithms.

Dataset enlargement includes the addition of the IDOR and Wallowa2 flex-array datasets to the preexisting data from the High Lava Plains and Wallowa1 flex-array deployments, the Transportable Array, and a few other small arrays. The most important tomographic improvements result from the use of 3-D ray tracing and the increased data density. Our goal is to provide more accurate images of the Pacific NW mantle structure, with a focus on the region in and around NE Oregon.

Previous tomography studies in this region identified two major high-velocity anomalies in the upper mantle beneath central Idaho and NE Oregon. Schmandt and Humphreys (2011) imaged a slab-like high-velocity structure extending to depths of 200–600 km beneath central Idaho and portions of adjoining states. They interpret this anomaly as a delaminated fragment of previously flat Farallon oceanic lithosphere abandoned during Siletzia accretion ∼50 Ma; its delamination is associated with the earliest termination of the Laramide orogeny and initiation of the ignimbrite flareup. Darold and Humphreys (2013) image the upper mantle Wallowa anomaly, located beneath NE Oregon. They suggest this anomaly was created by delamination of a flat fragment of Farallon lithosphere that was triggered by the arrival of Yellowstone to SE Oregon ∼16 Ma.

We image the Wallowa and central Idaho structures with greater resolution, finding them to be separate structures that may have somewhat separate histories. More regionally, two major low-velocity structures are imaged, as reported in previous publications. One is beneath eastern Snake River Plain (extending to ~180 km), and the other beneath the Cascadia backarc in central Oregon.

2. Data and methods

2.1. Data

Our model includes data from 315 broadband Transportable Array (TA) stations and multiple flexible array deployments (Fig. 1) that each collected ~2 years of data. Flex arrays include: Wallowa2 (33 stations, 2016–2018), IDOR (85 stations, 2011–2013), HLP (118 stations, 2006–2009), and other minor and legacy contributions from the compilation of Schmandt and Humphreys (2010b). Station spacing varies across the model, including ~75 km for the TA, 10–35 km for IDOR, 15–20 km for HLP, and 5 km for Wallowa2.

We use ~120,000 P and ~39,000 S delay times derived from events at 30–105° epicentral distance with $m_b > 5.5$ and additional delay times from steeply incident PKPdf and SKS phases (Fig. S1). Delay times were determined using multi-channel cross-correlation (VanDecar and Crosson, 1990). P-wave delays used in finite-frequency modeling are derived from four frequency bands: 0.5–1.5 Hz, 0.2–0.8 Hz, 0.1–0.5 Hz, and 0.04–0.16 Hz, with central frequencies of 1.0, 0.5, 0.3, and 0.1 Hz, respectively. S-wave delays are derived from three frequency bands: 0.1–0.7 Hz, 0.04–0.16 Hz, and 0.01–0.09 Hz, with central frequencies of 0.4, 0.1, and 0.05 Hz. The root mean square (RMS) of all P and S delay times before corrections is 0.42 s and 1.2 s respectively. The RMS of P delay times ranges between 0.40–0.44 s across all frequency bands. The RMS of S delay times are within 1.19 and 1.22 s.

The temperature and the presence of any partial melt in the shallowest mantle will have the greatest effects on velocity variation, and composition will have the least effect (e.g., Karato, 1993; Goes et al., 2000). Low temperature is thought to be the cause of seismically fast regions, while high temperature and partial melt create depressed velocities. To gain additional insight into these correlations, we use the slope of the best-fit linear regression of P and S delay times (Fig. 2) to estimate the integrated ray path $\partial \ln V_S / \partial \ln V_P$ (Hales and Doyle, 1967). This allows some understanding of how upper mantle V_P and V_S are affected by variations in temperature, anisotropy, composition, and the presence of partial melt. Neglecting the P and S ray-path geometry variations, we can estimate a depth average

$$\frac{\partial \ln V_S}{\partial \ln V_P} = \frac{\delta t_S}{\delta t_P} \frac{V_{S_0}}{V_{P_0}} \quad (1)$$

where δt_P and δt_S are the P and S delay times, and V_{P_0} and V_{S_0} are the depth average upper mantle velocities of our reference model (IASP91, Kennett and Engdahl, 1991).

The regression analysis takes into consideration the uncertainties associated with the P and S delay time measurements. Initially we use all delay times for common event-station pairs and calculate a slope of 2.86. If we assume a $V_P/V_S = 1.81$ for the upper mantle (IASP91) we obtain a $\partial \ln V_S / \partial \ln V_P$ of 1.58. In a second regression we ignore delay times slower than 1.5 s, which may well be influenced by the presence of partial melt, and calculate a slope of 2.14 corresponding to a $\partial \ln V_S / \partial \ln V_P$ of 1.18. Several studies indicate that temperature variations in the mantle can explain a $\partial \ln V_S / \partial \ln V_P$ ranging from 1.2 to 2 (e.g., Goes et al., 2000), based on assumptions about the attenuation structure. The western US mantle is characterized by high attenuation (Q_S of ~100,

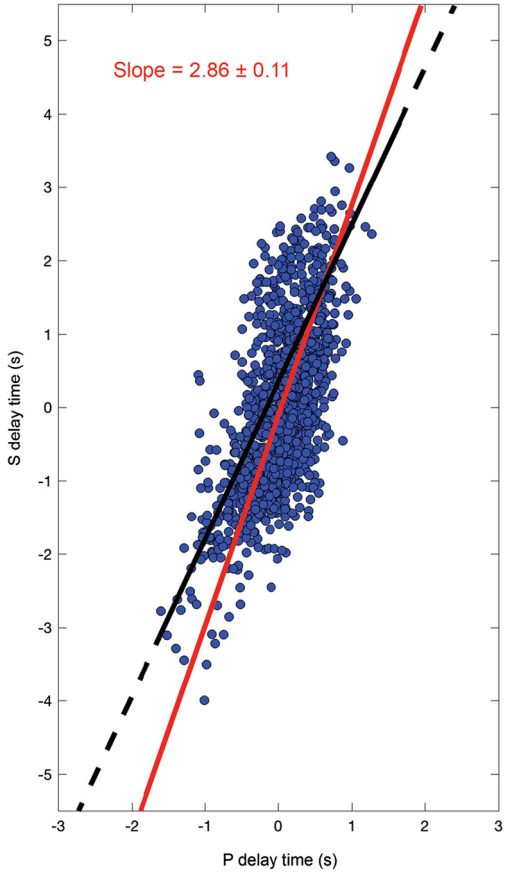

Fig. 2. Regression of P and S delay times for common event-station pairs. The best fitting line is plotted in red and has a slope of 2.86 with a standard error of 0.11. S uncertainty is assumed to be twice that of the P uncertainties. Black line (slope 2.14) ignores the times slower than 1.5 s, presumably influenced by partial melt.

e.g., Dalton et al., 2017), and Q_P can be approximated as $2.25 * Q_S$ (Knopoff, 1971) by assuming a Poisson solid and a large bulk modulus, therefore Q_S ~100 will scale to Q_P ~225. Using the scaling relations of Karato (1993) we find that our $\partial \ln V_S / \partial \ln V_P$ of ~1.2–1.6 is consistent with an interpretation of thermal variation.

2.2. Methods

To improve imaging of the upper mantle seismic structure beneath the Pacific NW interior, we incorporate a ray weighting algorithm to down-weight arrivals from common source areas, detailed calculations of crustal delay times, finite-frequency sensitivity kernels, and iterative 3-D ray tracing. The implementation of these advancements, and the addition of IDOR and Wallowa2 data to the existing TA and flexible-array data (Fig. 1), are each important for increasing model resolution. The most significant imaging improvements result from the additional data density and the use of 3-D ray tracing. In this section we describe our modeling process; more details about the methods and resolution tests are presented in the supplementary material.

High station density allows for a relatively fine model mesh in the uppermost mantle beneath the study region. The model space is parameterized with 10,935 nodes distributed on a 3-D rectangular grid extending from 0 to 590 km depth. Horizontal distance between nodes is 45 km, and vertical distance increases from 35–40 km at 0–350 km depth to 45–50 km at 350–590 km depth. Modeled slowness is linear between nodes. Prior to the inversion we apply event static corrections to remove the dependence of each event's average time on the particular set of stations that

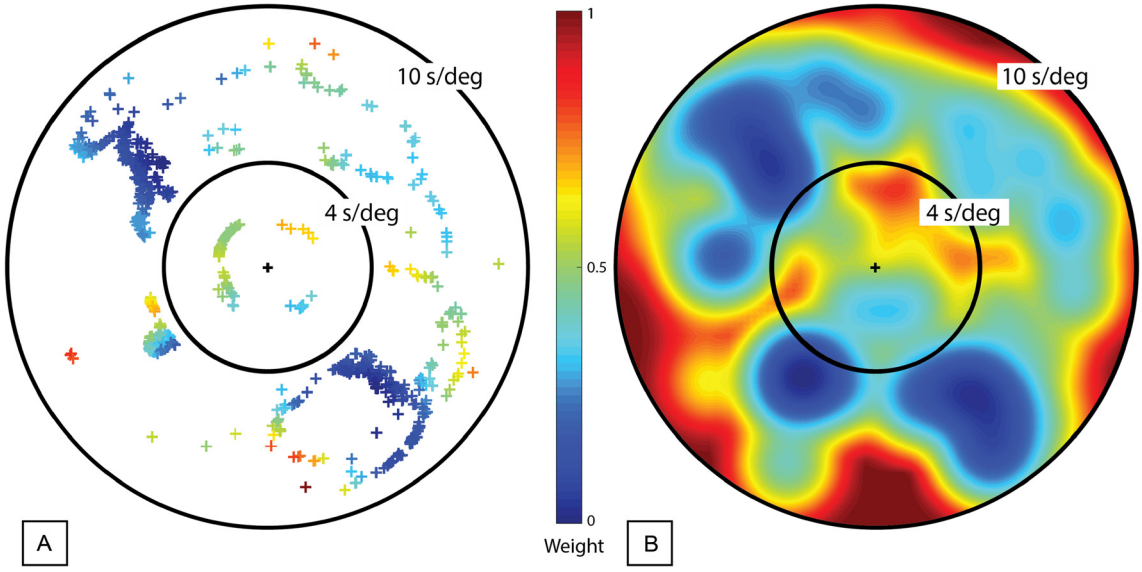

Fig. 3. (A) Distribution of incoming P rays plotted in the ray-parameter – back-azimuth space. Color indicates assigned ray weight, obtained from (B). (B) Ray weight function, calculated from the local ray density in the ray-parameter – back-azimuth space. Arrivals slower than 4 s/deg are core phases.

recorded that event. This accounts for the fact that the average arrival time of each event varies depending on Earth structure outside of our model volume and errors in event origin parameters. We account for various arrays operating at different times and in different geologic settings by applying an array time correction following the method of Humphreys and Dueker (1994). We find that differences between average arrival times across all arrays are generally small, for example, 1 Hz P rays are <0.1 s. The exceptions are Wallowa1 and HLP, which are ~0.2 s.

The inverse problem is solved using the LSQR damped least-squares method (Paige and Saunders, 1982). For the P and S inversions we minimize the cost function

$$\boldsymbol{\varepsilon} = \|\boldsymbol{G}\boldsymbol{m} - \boldsymbol{d}\|^2 + \lambda_{\mathrm{m}}\|\boldsymbol{m}\|^2 + \lambda_{\mathrm{L}}\|L\boldsymbol{m}\|^2 + \lambda_{\mathrm{D}}\|D\boldsymbol{m}\|^2 \quad (2)$$

where $\boldsymbol{G}$ is the sensitivity matrix, $\boldsymbol{m}$ is the model vector, $\boldsymbol{d}$ is the data vector (with crustal and elevation travel-time corrections made). λ_{m}, λ_{L}, and λ_{D} are the weights for the norm damping term, the Laplacian smoothing matrix L, and the edge damping term D, respectively. This last term is a diagonal matrix that damps the top 55 km of the model, which is incorporated with the crustal corrections.

The joint $V_{\mathrm{P}}/V_{\mathrm{S}}$ inversion minimizes the cost function in Equation (3). We simultaneously invert for V_{P} and V_{S} and use Equation (5) to calculate the final model.

$$\boldsymbol{\varepsilon}_{\boldsymbol{V_P/V_S}} = \boldsymbol{\varepsilon}_{\boldsymbol{V_P}} + \mathrm{b}\boldsymbol{\varepsilon}_{\boldsymbol{V_S}} + \lambda_{\boldsymbol{V_P/V_S}}\|L_{\boldsymbol{V_P/V_S}}\boldsymbol{m}_{\boldsymbol{P,S}}\|^2 \quad (3)$$

where $\boldsymbol{\varepsilon}_{\boldsymbol{V_P}}$ and $\boldsymbol{\varepsilon}_{\boldsymbol{V_S}}$ are the individual cost functions for P and S inversions and $\lambda_{\boldsymbol{V_P/V_S}}$ is the weight applied to the regularization term. The relative weights of the P and S data sets are kept equal by scaling V_{S} with a factor b = 1.8. This value is chosen such that

$$\mathrm{b} = \|\boldsymbol{d_P}\|/\|\boldsymbol{d_S}\| \quad (4)$$

We regularize the inversion using a gradient operator described in Equation (E3) (e.g., Hammond and Toomey, 2003). We simultaneously impose smoothness constraints on $\delta \ln V_{\mathrm{P}}$, $\delta \ln V_{\mathrm{S}}$, and $\delta \ln V_{\mathrm{S}}/\delta \ln V_{\mathrm{P}}$. We use a reference $V_{\mathrm{P}}/V_{\mathrm{S}}$ (from IASP91) to constrain the final model, which becomes

$$\delta \ln \left(\frac{V_{\mathrm{S}}}{V_{\mathrm{P}}}\right) = \frac{\delta \ln V_{\mathrm{P}} + 1}{\delta \ln V_{\mathrm{S}} + 1} - 1 \quad (5)$$

where $\delta \ln V_{\mathrm{P}}$ and $\delta \ln V_{\mathrm{S}}$ are the jointly resolved P and S models.

2.2.1. Ray weighting

A teleseismic ray set is highly heterogeneous in back-azimuth and ray parameter distribution (Fig. 3). We down-weight rays of relatively common ray parameter and back-azimuth to minimize the inherit streaking created by corridors of high ray density (Fig. 3). A weighting function in ray parameter – back-azimuth space is made from our ray set, using the ray parameter and back-azimuth of each event to our array center. The ray parameter – back-azimuth space is meshed and the weight for each 0.25° × 0.25 s/km cell is calculated with

$$w_n = 1 - \frac{\ln(N+1)}{\max(N)} \quad (6)$$

where w_n is the weight given the nth cell, and N is the number of rays per cell (Fig. 3). The weight of each ray to each station is found by interpolation in the weighting function.

2.2.2. Crustal and elevation corrections

The upper ~55 km of a tomographic mantle model are generally poorly resolved due to the lack of ray crossings as the incidence angle is close to vertical and station path convergence. Accurately resolving the upper mantle portion of the delay time depends on having an accurate estimate of the crustal travel time. This is particularly important as the choice of crustal corrections can artificially affect the imaged amplitude of mantle seismic anomalies. Fig. S8 shows how crustal model choices affect the tomography results. The effects are small but noticeable at shallow mantle depths. Crustal corrections should prevail over the use of station statics, which are less precise and could lead to misallocation of the mantle delays, however estimating crustal delay times is dependent upon the availability of well-resolved crustal models.

We construct a high-resolution velocity model of the crust and uppermost mantle to a depth of 55 km that uses published results derived from Rayleigh waves and controlled-source studies (Fig. S7). We use Shen and Ritzwoller (2016) crustal velocity model, sampled at 0.25° × 0.25°, as our background model, into which we integrate higher-resolution crustal models from Davenport et al. (2017), Cox et al. (2013), and Lerch et al. (2007), and a Moho surface derived from regional receiver functions studies (Shen et al., 2013; Gao, 2015; Stanciu et al., 2016). At each station,

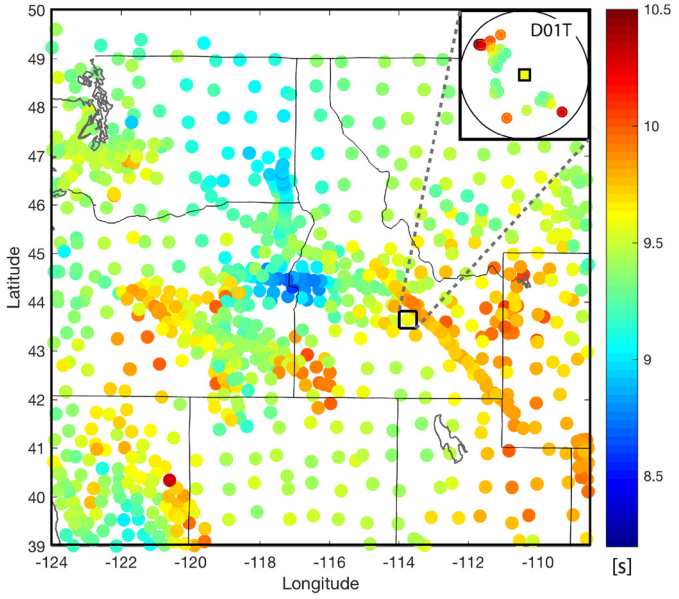

Fig. 4. Station correction average time (seconds) for P rays for the stations used in our study. Included in these calculations are crust and mantle velocity structure to 55 km (from Shen and Ritzwoller (2016) and various crustal studies discussed in the supplementary material, Fig. S7). Inset shows station D01T crustal times plotted in ray-parameter – back-azimuth space.

topography is included as a layer of velocity 5.0 km/s for P and 2.9 km/s for S and thickness based on station elevation. The travel times calculated through this composite model are subtracted from the ray's delay time. Fig. 4 shows the resulting station-average P delay times. Reasonable choices of crustal model result in small changes in upper mantle seismic structure that can be evident to depths of 100 km (Fig. S8). The RMS of P and S crustal time corrections are 0.11 s and 0.19 s respectively. After all corrections are applied, the RMS of the P and S delay times are reduced from 0.42 to 0.38 s and from 1.2 to 1.1 s.

2.2.3. Finite-frequency effect

We incorporate finite-frequency sensitivity kernels ("banana-doughnut"), as described in Dahlen et al. (2000) and approximated by Schmandt and Humphreys (2010a). We calculate the sensitivity kernel along the 3-D ray path at each depth interface for each of the overlapping frequency bands (1, 0.5, 0.3, and 0.1 Hz central frequencies for P and 0.4, 0.1, and 0.05 Hz for S) and stack these in the $\boldsymbol{G}$ matrix. In all iterations, the frequency-dependent kernels are conformed to the ray path, i.e., at each depth the center of the sensitivity kernel is located at the ray position. The corresponding delays are stacked in the data vector $\boldsymbol{d}$. The differences in P seismic structures imaged with finite-frequency kernels are minor compared to inversion using ray theory approximation (Fig. 5), because the finite-frequency inversion is dominated by data in the 1 Hz frequency band, which has finite-width sensitivity kernels that are narrow compared to model node spacing. The effect is more pronounced on S seismic structures because the S wave frequency bands result in Fresnel zones wider than the node spacing. For example, the first Fresnel zone radius for a 1 Hz P ray increases from ∼28 to ∼50 km between 100 and 300 km depth. For a 0.1 Hz S ray, the radius increases from ∼66 to ∼117 km over the same depth range.

2.2.4. 3-D ray tracing

Teleseismic ray tracing in an Earth with velocity depending solely on depth will mislocate the ray position where a ray encounters a horizontal gradient in velocity, because the ray minimum-time path tends to bend towards higher velocities. The result is an over-estimation of the width of high-velocity structures and underestimation of the width of low-velocity structures.

Our ray-tracing algorithm uses a 1-D velocity model to calculate travel times outside our model box and a 3-D model for travel times inside the box. Rays are traced using IASP91 to the boundary of the inversion box, and traced in 3-D through the intermediary velocity model (from the previous iteration) within the box. Box penetration location is chosen such that net travel time is minimized (see supplementary material). The updated velocity structure is then used as the reference velocity in the next iteration. In practice, model improvement is negligible after one iteration of ray tracing and we have applied no additional iterations. Data variance is reduced by 10–15% relative to inversion using only 1-D ray tracing. The improved imaging of steeply dipping high-velocity structures results in a ∼10% thickness reduction in the horizontal direction (Fig. 6).

3. Results

Of the upper mantle imaged by USArray, no region has more major fast and slow velocity structures than the Pacific NW. These structures are large in volume and strong in magnitude. They tend to define coherent entities, although in some places it is not clear what to include or exclude when defining a given structure. Previous work has identified and suggested origins for most of these anomalies (e.g., Schmandt and Humphreys, 2011; Darold and Humphreys, 2013). The purpose of this paper is to better define and describe these structures.

Throughout the model space the P and S structures are consistent with one another and negatively correlated with the V_P/V_S structures (Figs. 7–9). The main differences between the P and S datasets result from different numbers of available ray paths and different frequency ranges for measuring the P and S delay times. The P and S seismic structures are strongest in the top 300 km and 200 km of the model respectively. The V_P/V_S model amplitudes are similar to those resolved in the P model. Discrepancies in P and S model heterogeneities (Figs. 7–8) primarily occur below 200 km, where S amplitudes decrease significantly compared to P.

3.1. Wallowa anomaly

The Wallowa seismic structure beneath the Wallowa Mountains in NE Oregon is prominent in both P and S-wave images (WA, Figs. 7–8) and it is not as well defined in the V_P/V_S model (Fig. 9). It lies beneath the NE end of the accreted Mesozoic Blue Mountains terranes, which are bounded on the north and east sides by the $^{87}Sr/^{86}Sr$ 0.706 isopleth that indicates the presence of Precambrian crust to the north and east of the Blue Mountains' suture to North America. We image the Wallowa anomaly to depths of 300–350 km. Below 150 km it is 3% fast in the P image and 5.5% fast in the S model (Figs. 7–8). Cross section through the P model show a SSE dip at ∼10° (Fig. 10). This structure may end above 100 km, or it may connect to the overlaying North American lithosphere in a location ∼100 km west of the deeper structure. Darold and Humphreys (2013) attributed this anomaly to a fragment of Farallon slab that was left flat against the base of the Blue Mountains ∼50 Ma and delaminated during the Columbia River flood basalt event ∼16 Ma.

3.2. Idaho curtain

The central Idaho seismically fast structure, the "Siletzia anomaly" of Schmandt and Humphreys (2011), is a north-oriented structure located east of the Wallowa anomaly (IC, Figs. 7–8). It lies entirely beneath Precambrian crust and extends from the base of

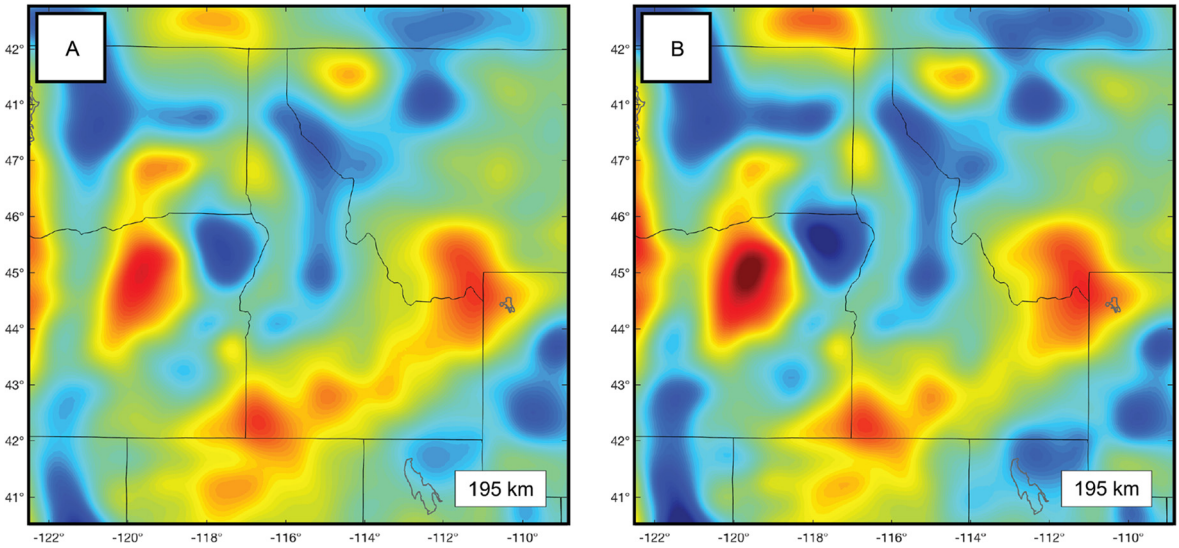

Fig. 5. Comparison between ray-theoretical (A) and finite frequency (B) inversions. Same regularization is used in both cases and the inversions do not include the 3-D ray-tracing effects.

the crust to ~400 km depth (Figs. 7, 10). Although larger in volume than the Wallowa anomaly, it is not as anomalously fast, less than 3%, as resolved by our P and S inversions. A possible continuation of this structure trends west across northern Washington at depths of 125–270 km in the P model (Fig. 7). While this potential connection is not resolved in the S model, an E-W anomalous structure is indicated by the V_P/V_S model (Fig. 9).

3.3. Seismically fast structure beneath the Atlanta lobe of the Idaho Batholith

The P imaging shows a relatively small structure of 1–2% elevated velocity located south of the central Idaho anomaly, beneath the southern region of the Atlanta lobe and a neighboring portion of the Snake River Plain. This structure extends from the base of the crust to ~100 km depth (IB, Fig. 7). Due to its shallow depth, the shape and magnitude of this structure are sensitive to the choices made during model regularization, but its presence at this location is persistent through all our modeling efforts. This structure may or may not be a part of the nearby central Idaho anomaly. The S and V_P/V_S models do not resolve this structure well.

3.4. Slow anomalies

There are two prominent low-velocity structures in our model, and several lesser slow structures. The slow mantle beneath the eastern Snake River Plain (SRP)–Yellowstone system (SRP-Y, Figs. 8–10) is the most prominent slow structure above 190 km. Our models resolve the SRP–Yellowstone structure between the base of the crust and 165–190 km depth.

A major slow anomaly is present beneath north-central Oregon, extending from ~160 km to 270 km depth. In this depth range, it is the slowest structure in the Pacific NW. The seismic amplitude of the north-central Oregon structure at 200 km depth is ~3% slow in the P and S model (S1, Figs. 7, 8) and less than 3% fast in the V_P/V_S model (Fig. 9).

At shallow depths, above 100 km, we resolve a distinct slow anomaly (~2%) across the Oregon-Idaho border centered at 44° N and -117° E (S2, Figs. 7, 10). This location is within the footprint

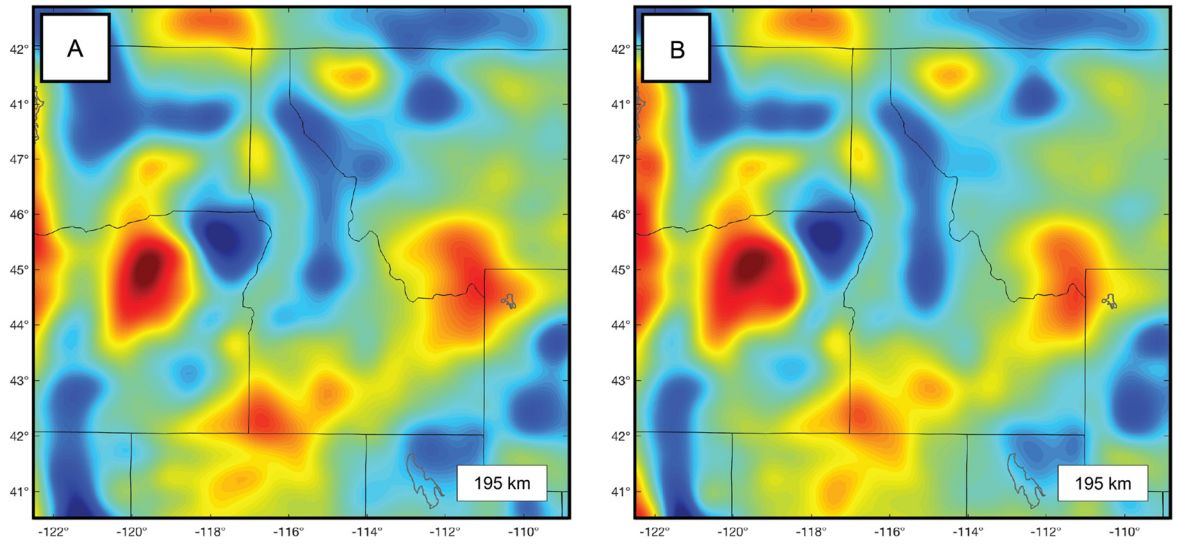

Fig. 6. Improved P tomography from 3-D ray tracing. (A) inversion results before ray tracing; (B) inversion results with ray tracing. Note that fast anomalies tend to get thinner. The same regularization is used in both inversions.

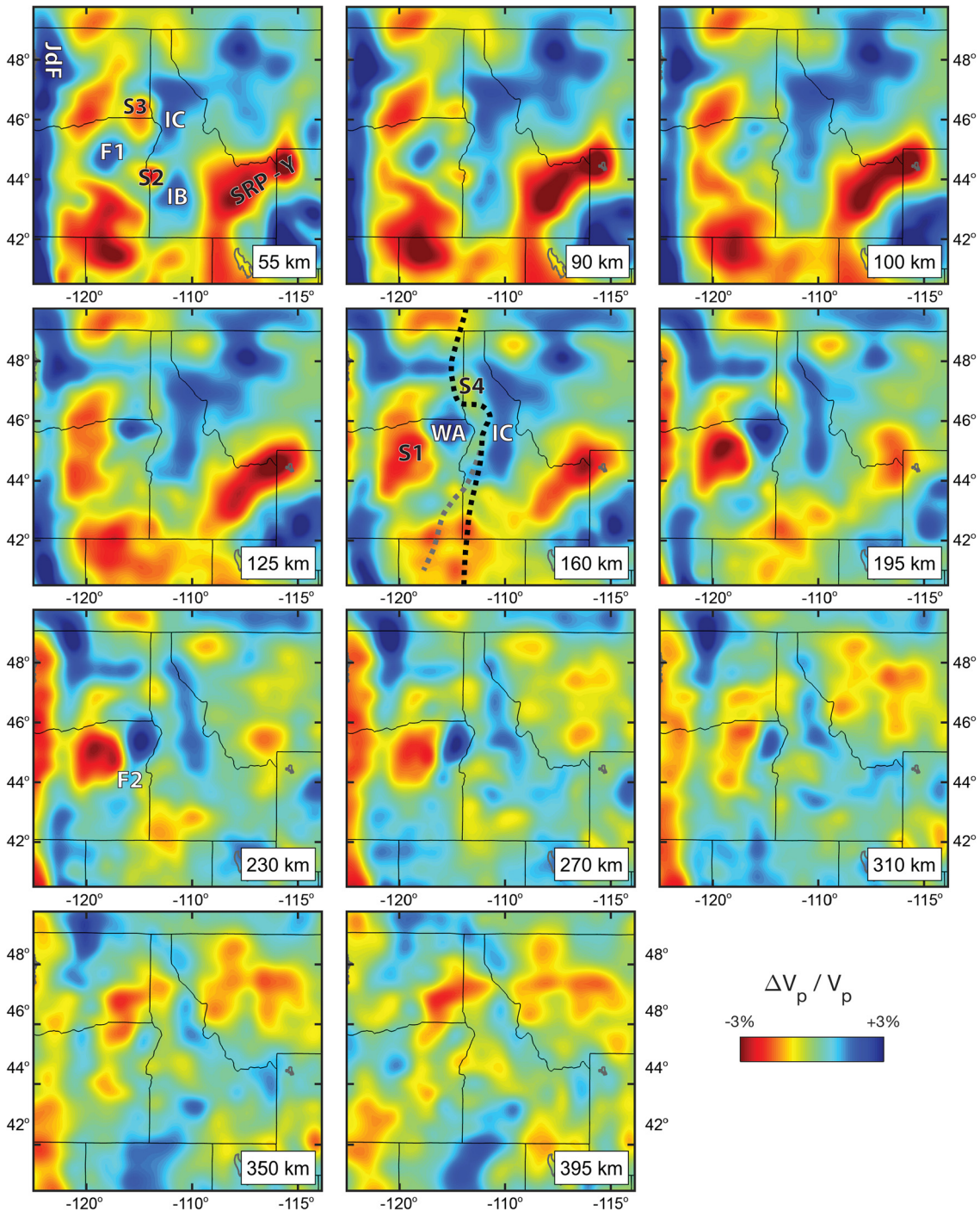

Fig. 7. Upper mantle P tomography depth slices. Colors represent velocity perturbations. V_P seismic structures have strongest amplitude in the upper 200 km. Black and grey dashed lines show the location of the $^{87}Sr/^{86}Sr$ 0.706 and 0.704 isopleths. Seismically fast structures: JdF: Juan de Fuca slab; WA: Wallowa anomaly; IC: Idaho curtain anomaly; IB: Idaho batholith anomaly; F1: north-central Oregon fast anomaly; F2: eastern Oregon anomaly. Seismically slow structures: SRP-Y: Snake River Plain-Yellowstone anomaly; S1: north-central Oregon slow anomaly; S2: Oregon-Idaho border anomaly; S3: Oregon-Washington border anomaly; S4: Washington-Idaho border anomaly. Wallowa and the Idaho curtain anomalies are separated at depth throughout the model space.

of the Yellowstone mantle plume head impact where Wolff et al. (2008) propose the location of a large crustal magma chamber that fed the lavas of the Columbia River flood basalts. A second shallow slow structure (S3) is resolved across the boundary between Oregon and Washington, which extends to depths of ~100 km. Neither of these structures is resolved by the S and V_P/V_S models.

An ~1% slow seismic heterogeneity is imaged in the P model in the 160–270 km depth range, immediately south of a break in the E-W segment of the Idaho seismic anomaly (S4, Fig. 7). This structure is not well resolved in the S model.

3.5. Other lesser seismically fast velocity heterogeneities in the Pacific Northwest interior

Much of the Cascadia backarc is slow to ~160 km depth, especially beneath NW Nevada. This low-velocity structure often extends a few hundred kilometers east of the Cascade arc, and it is not simple along strike.

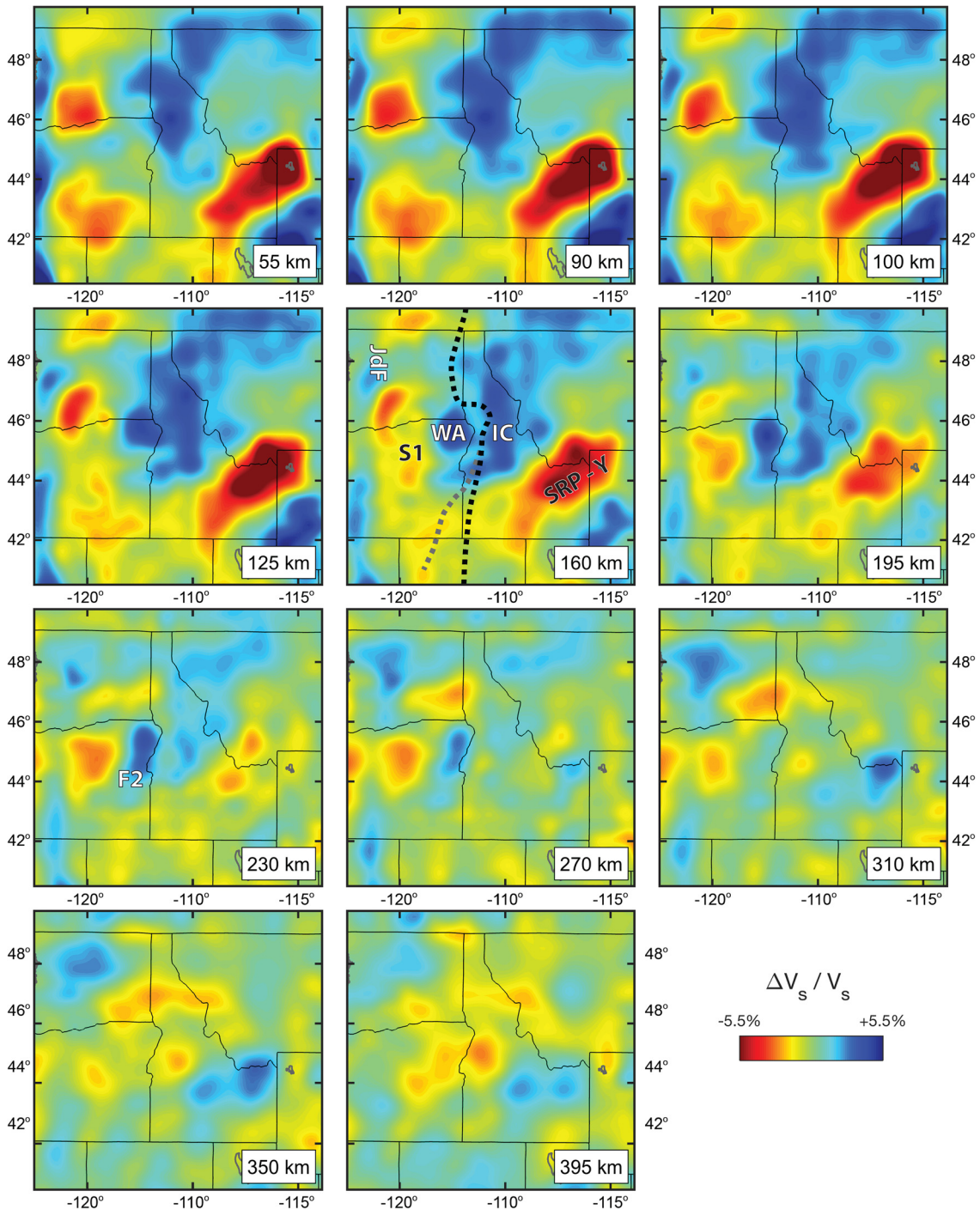

Fig. 8. Upper mantle S tomography depth slices. Black and grey dashed lines show the location of the $^{87}Sr/^{86}Sr$ 0.706 and 0.704 isopleths. Seismic structures: JdF: Juan de Fuca slab; WA: Wallowa anomaly; IC: Idaho curtain anomaly; F2: eastern Oregon anomaly; SRP-Y: Snake River Plain-Yellowstone anomaly; S1: north-central Oregon slow anomaly.

We resolve several upper mantle structures >1% faster than the average asthenosphere located west of central Idaho (Fig. 7). As high-velocity structures they are thought to be relatively cool. Because they lie in the forearc of the Cretaceous arc, it seems unlikely they represent foundered North American lithosphere, and hence we think these structures are slab fragments. Cumulatively, these could explain some of the many thousands of km of Juan de Fuca slab that are missing down-dip of the slab we resolve today above 400 km. Alternatively, they could be fragments associated with the westward step of subduction zone that occurred during Siletzia accretion.

We image a seismically fast structure in the 55–90 km depth range beneath north central Oregon (near -119°E and 45°N) that is west of the Wallowa anomaly (F1, Fig. 7). It is located approximately above the slow anomaly imaged in the 160–270 km depth range. It does not appear to be connected with any of the deeper fast structures, but it's strength and proximity to the Wallowa anomaly suggests a possible relation. This structure is less resolved by the S model, where it is observable at an amplitude of <1%.

Beneath eastern Oregon, in the 270–400 km depth range, we observe an irregularly shaped low amplitude ~1% seismically fast structure roughly connecting the Wallowa anomaly to the southern

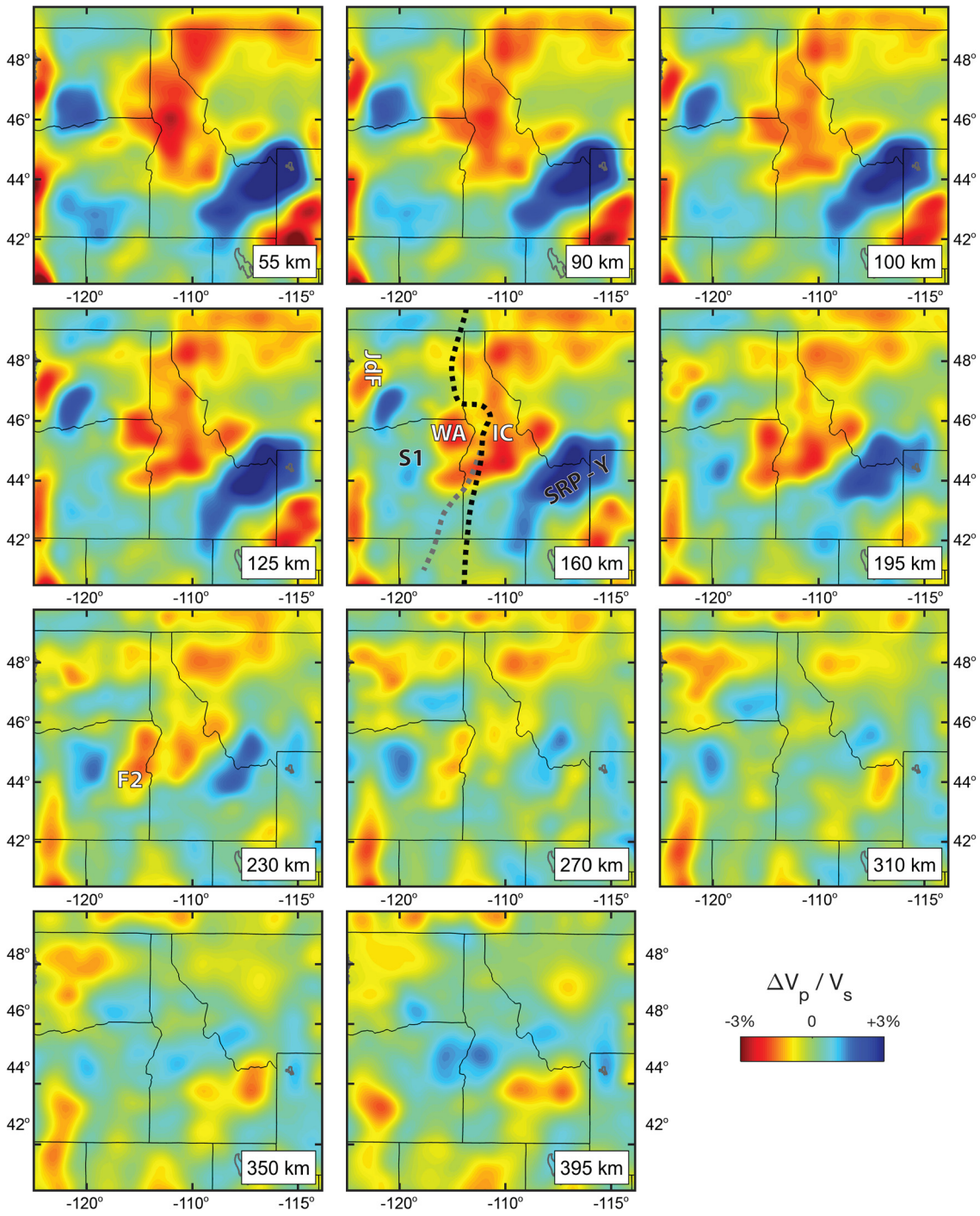

Fig. 9. Depth slices through the V_P/V_S model. Seismic structures: JdF: Juan de Fuca slab; WA: Wallowa anomaly; IC: Idaho curtain anomaly; F2: eastern Oregon anomaly; SRP-Y: Snake River Plain-Yellowstone anomaly; S1: north-central Oregon slow anomaly.

Oregon Juan de Fuca slab, and effectively defining the southern boundary of the central Oregon slow anomaly (F2, Figs. 7–9). While clearly resolved in both P and S models, we can only trace it down to about 300 km in the S and Vp/Vs models.

4. Discussion

The Pacific NW is exceptional for its complex Cenozoic geologic history, distinct from British Columbia to the north or California to the south. The diversity of tectonic and magmatic events includes a subduction jump following Siletzia accretion and magmatism occurring nearly everywhere in the region, including arc initiation, ignimbrite flareup, and Columbia River flood basalt eruptions (Fig. 1). How these events are related to one another is not well understood, and mantle structures provide important constraints on this history.

4.1. Physical state of Pacific Northwest interior upper mantle

The factors that can affect upper mantle seismic velocity variations are temperature, composition, anisotropy, and the presence of partial melt (e.g., Karato, 1993; Goes et al., 2000). Composition has little effect in the upper mantle (e.g., Lee, 2003; Schutt and Lesher, 2006). Velocity perturbations that are more than 1% faster than

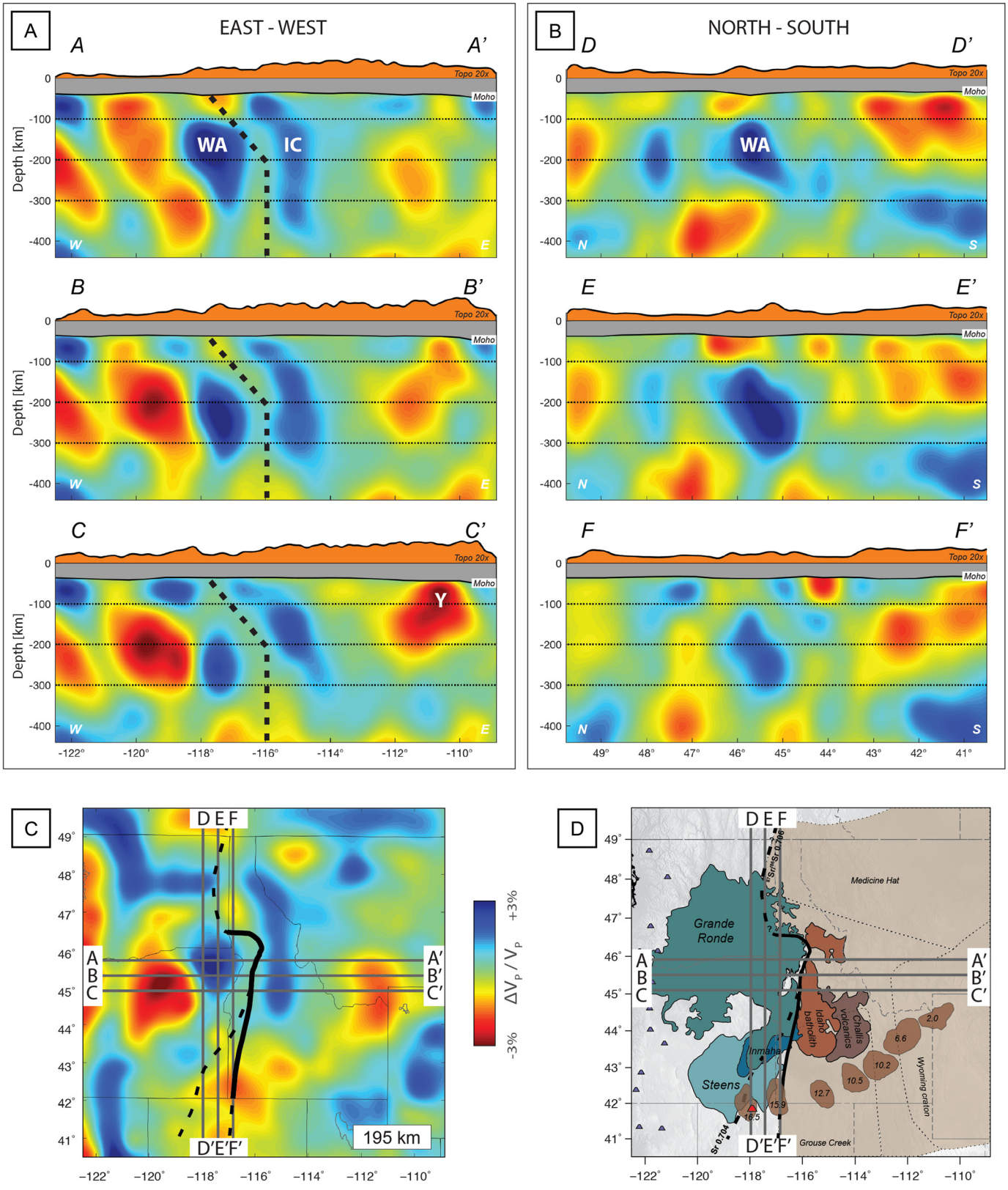

Fig. 10. (A) E-W cross-sections through the P tomography model showing the lateral separation of Wallowa and Idaho curtain anomalies (emphasized with a black dashed line); Location of the profiles is shown in (C) and (D); (B) N-S cross-sections through the Wallowa anomaly, as imaged in the P tomography model. (C) 195 km depth P tomography section; (D) map with the main geological features (for details see Fig. 1).

average are attributed to relatively cool temperatures. At 200 km depth, Cammarano et al. (2003) estimate the anharmonic effects of cooling by 100 °K leads to a respective 0.7% and 1.25% increase in P and S velocity. Relatively low upper mantle temperatures are created near the surface, and when they are found below the lithosphere it is inferred they descend into the upper mantle. Because most of our study area was forearc continent prior to ∼50 Ma, we do not expect thick continental lithosphere in this region. Hence,

the imaged high-velocity structures are thought to be fragments of oceanic lithosphere, such as Farallon ocean lithosphere. Assuming temperature effects alone, a 3% fast upper mantle V_P structure could represent a 400 °C lateral variation in temperature.

Anomalously slow upper mantle is usually associated with anomalously hot mantle and can indicate the presence of partial melt. The sensitivity of seismic velocity on temperature increases with temperature because of the increasing effect of anelasticity. At 200 km depth, the temperature derivatives of seismic velocity increase by about 50% (Cammarano et al., 2003). In addition, higher temperatures can create partial melt, especially in the presence of vapor. Hammond and Humphreys (2000) calculate the effect of 1% partial melt on mantle velocity to represent a reduction of about 3.6% and 7.9% in P and S wave velocity, respectively. In our model area, regions of very low velocity and large V_P/V_S that are consistent with the presence of partial melt are Snake River Plain and central Oregon anomalies.

4.2. Complex subduction and outstanding questions the imaged structure informs

We image three prominent and several minor high-velocity upper mantle structures. The tectonic evolution of the PNW is thought to require each of the three major structures to be subducted ocean lithosphere (Schmandt and Humphreys, 2010b; Darold and Humphreys, 2013). In the western part of our study, between -122°E and -121°E, the subducting Juan de Fuca slab is easily identified to depths of ∼300 km. To the east, the Idaho curtain is thought to be Farallon lithosphere that foundered ∼50 Ma. If so, it has resided stably near its present location for this duration, a feat attributed to young slab age (modest negative buoyancy), the depleted (buoyant) nature of ocean lithosphere, and the inevitable loss of stalled slab crust. In the center of our study region, the Wallowa anomaly is found to be structurally distinct from the Idaho curtain. This lithosphere is thought to have delaminated from the base of North America ∼16 Ma (Darold and Humphreys, 2013). Its seismic strength is greatest at ∼250 km depth. Directly above the strong seismic anomaly, its seismic strength diminishes greatly, and at shallower depths it appears to join with high-velocity mantle 150 km to the southwest (Fig. 7). The overall sense we get for these high-velocity structures beneath the Pacific NW interior is one in which much of the subducted Farallon left flat against the base of North America during the Laramide orogeny has foundered since occurrence of the eastward jump in subduction that initiated Cascadia.

A minor high-velocity structure extends to depths of ∼100 km beneath the Atlanta lobe of the Idaho Batholith, and the Snake River Plain low-velocity anomaly arcs south of this structure. Possible explanations for the Atlanta lobe structure include a preserved fragment of North America lithosphere, or a fragment from the Cretaceous slab associated with the initial emplacement of the Idaho Batholith (Gaschnig et al., 2011).

Several seismically slow bodies are present beneath the PNW. Beneath the eastern Snake River Plain (but not western Plain), the upper mantle is very slow to depths of ∼170 km. The upper mantle is slow in much of the Cascades back arc; beneath the shallow northern California back arc it is very slow, as it is beneath the deep (180–250 km) northern Oregon back arc. As one follows this structure to depths of ∼400 km, it trends to the northeast into a region beneath east-central Washington.

The strong slow anomaly beneath north-central Oregon is the deepest anomaly slower than 2% yet imaged beneath the U.S. Ideas for its origin include remnants of the hot Yellowstone plume drawn NW by oblique subduction (e.g., Draper, 1991; Kincaid et al., 2013), and eastward flow of hot asthenosphere through a tear in the Juan de Fuca slab (Hawley and Allen, 2019) (Figs. 7–8). Normal scaling relations suggest these entities owe their origin to elevated temperature and the presence of interstitial melt. At these depths, the presence of CO_2 is inferred to be the primary driver for melt generation (Dasgupta et al., 2013). The deep Oregon anomaly can be attributed to melting of carbonated peridotite in the presence of oxidizing conditions and elevated temperatures at depths of ∼300 km (e.g., Dasgupta et al., 2013; Villagómez et al., 2014).

4.3. Northeast Oregon and the Columbia River flood basalts

The 16 Ma Columbia River basalt (CRB) eruptions covered most of eastern Oregon and extensive regions of Idaho and southern Washington (Fig. 1). Both bottom-up and top-down processes have been put forward to explain the origin and evolution of these eruptions. The bottom-up processes are based on the ∼17 Ma Yellowstone plume arrival at the base of North America somewhere beneath north-central Nevada to east-central Oregon, initiating volcanism at McDermmitt caldera and the Steens Mountain area (Fig. 1). Flood basalt chemistry has a plume signature, often mixed with depleted mantle lithosphere and, for the Grande Ronde lavas, Archean crust (Wolff and Ramos, 2013). However, a plume-only model does not explain for the northward propagation of the CRB eruptions, the associated increasing volume of erupted lava, or the creation of kilometer-scale uplift in northeast Oregon, where some of the largest eruptions occurred.

Top-down processes incorporate the foundering of gravitationally unstable lithosphere (Hales et al., 2005) or extension-induced localized melting of the upper mantle (e.g., Hooper et al., 2002). While Wolff et al. (2019) argue that the absence of a deep-seated upwelling mantle signature (lack of magnesium-rich melt), and the presence of subduction-related chemical signature (LILE enrichment) are evidence against a mantle plume, they propose a reconciliation of the geochemical signatures with a hybrid model that includes both regional lithospheric instabilities and plume upwelling. Similarly, our preferred model for the CRB (from Darold and Humphreys, 2013) includes the impingement of Yellowstone plume from below, which triggered northward-delamination of the Farallon lithosphere lying flat against eastern Oregon before 17 Ma. Farallon slab rollback beneath NE Oregon enabled Wallowa root foundering. Our imaging of upper mantle structure beneath Oregon and central Idaho is consistent with the previous tomographic studies, but the improved resolution provides the basis for a more specific interpretation.

4.4. Wallowa anomaly

The Wallowa seismically fast anomaly was interpreted by Darold and Humphreys (2013) to be Farallon lithosphere that delaminated from south to north beneath the base of North America, driving the evolution of the CRB. Our new imaging brings three new constrains: (a) the Wallowa anomaly is nearly or completely separated from the overlying lithosphere, (b) there is a clear separation between Wallowa and central Idaho seismic structures, and (c) this separation coincides with the Precambrian margin of North America. Because the high-velocity Wallowa anomaly appears only weakly connected to high velocity mantle above 100 km and ∼150 km to the SW (Figs. 7, 10), we propose that the Wallowa anomaly is detached, or currently detaching, from the overlying lithosphere. The separation between the Wallowa and Idaho curtain anomalies could indicate an independent origin and physical nature of the two structures. And the striking correlation with the western edge of Precambrian North America – as defined by $^{87}Sr/^{86}Sr$ 0.706 isopleth (Fig. 7, 10) – suggests a control of the Precambrian North American margin during foundering of the Wallowa anomaly from the base of North America.

4.5. Physical origin of the Wallowa and Siletzia anomalies

Compared to the high-velocity Idaho curtain, the Wallowa structure has higher amplitude and is more compact in shape (Fig. 10). The two neighboring structures are spatially separated from one another from the base of the crust to their terminations at depth (Fig. 10). Synthetic resolution tests (supplementary material, Fig. S2) indicate that we can resolve a vertical gap that is 50 km wide between these structures. This vertical separation coincides with the Precambrian margin of North American craton along the $^{87}Sr/^{86}Sr$ 0.706 isopleth. Depending on the location of the spreading center between the Kula/Resurrection and Farallon plates at ~65–55 Ma, this juxtaposition is consistent with either of two general scenarios. (1) The Wallowa and Idaho structures have different origins, e.g., the Idaho anomaly is a fragment from the southern part of the Kula or Resurrection Plate, while Wallowa originated from the northern end of the Farallon plate. (2) Alternatively, these anomalies could represent fragments of the same plate that have been disrupted by subsequent tectonic deformation such as Siletzia accretion, Pacific NW rotation or delamination of the Wallowa or central Idaho slabs. The northward delamination and roll back of the flat Farallon plate could have occurred along the edge of the Precambrian craton margin, independent of the Idaho anomaly. This is consistent with the separation we image between the seismic structures along the edge of the margin, and the great difference in time of the volcanism that we think is associated with slab foundering. Our model indicates the Wallowa structure could be detached or in the process of detaching from the overlying lithosphere.

We infer that PNW tectonism and volcanism involves both the sinking of the negatively buoyant imaged high-velocity structures, including the subducting Juan de Fuca slab and earlier foundering of ocean lithosphere that was abandoned beneath the region (e.g., Wallowa and central Idaho structures), and the ascent of asthenosphere. Upward asthenospheric flow has been driven both passively by the sinking negatively buoyant lithosphere and actively by positively buoyant asthenosphere delivered by the Yellowstone plume. In addition, active (positively buoyant) asthenosphere ascent has played an important role in the PNW with the arrival of the Yellowstone plume. In our study area, this ensemble of small-scale buoyancy-driven flow fields interact to create a rather complex convective system as destabilized lithosphere adjusts and organizes to both the new tectonic setting and the passage of a plume.

5. Conclusions

We improve upper mantle seismic imaging beneath the Pacific Northwest interior by employing a combination of new data and improved techniques. We resolved reduced horizontal thickness of high-velocity structures and identify new anomalies. Following are the main conclusions.

(1) Improved upper mantle tomography model. Our imaging incorporates data from USArray-TA stations, flexible-array experiments, and the recent Idaho-Oregon and Wallowa2 deployments. We employed improvements in tomographic techniques, including ray-geometry weighting, careful calculation of crustal delay times, 3-D ray-tracing, and finite-frequency effects.
(2) Wallowa–Idaho curtain separation and characteristics. A clear separation between the Wallowa and Idaho anomalies occurs beneath the Precambrian margin of North America. These two structures have different shapes and seismic amplitude. This suggests these structures have different origins, e.g., the Idaho anomaly is a fragment of the Kula plate, and the Wallowa anomaly is a fragment of Farallon; alternatively, they could be pieces of the same plate that have experienced different tectonic histories during or after fragmentation.
(3) Fast velocity structure beneath the Atlanta lobe of the Idaho Batholith. We envision several origins for the fast velocity structure beneath the Atlanta lobe of the Idaho Batholith: a remnant from the Cretaceous slab responsible for the formation of the initial phase of Idaho Batholith, a fragment related to the deeper Idaho anomaly, or a preserved fragment of thick North American lithosphere.
(4) Slow anomaly east of the Juan de Fuca slab gap**.** An unusually large, deep and slow anomaly occupies the volume in the 160–270 km depth range immediately east of the Juan de Fuca slab. At this depth range, this structure is slower (and presumably hotter) that any structure beneath the Pacific Northwest, including Yellowstone. This anomaly may be plume mantle, either from Yellowstone's arrival beneath SE Oregon or that accumulated beneath the Juan de Fuca ocean plate and flowing through the Juan de Fuca slab gap.
(5) Other fast velocity heterogeneities in the Pacific Northwest interior. We image several structures >1% faster that average asthenosphere. We suspect these are slab fragments related to the region's evolving subduction history, and may account for the thousands of kilometers of Juan de Fuca slab that is not found downdip of the slab imaged above 400 km.

The refined geometries and amplitudes of Pacific Northwest seismic structure improve the potential for determining the origins of lithospheric fragments in the mantle and are key elements for reconstructing the evolution of the Pacific Northwest-Farallon-Kula-Juan de Fuca tectonic system.

Declaration of competing interest

The authors declare that they have no known competing financial interests or personal relationships that could have appeared to influence the work reported in this paper.

Acknowledgements

We thank Kathy Davenport, Haying Gao, Randy Keller, and Derek Lerch for providing crustal velocity models. We thank Raymond Russo, Victor Mocanu, Robert Clayton, and Kirsten Nicolaysen for making the IDOR and Wallowa2 flexible array experiments possible. We thank Pat Ryan, Richard Guy, Jonathan Perry-Houts, Jorge Castellanos, Nick Wogan, and Gabe Juul for their help with the data acquisition during the Wallowa2 experiment. The seismic data used in this study are available through the IRIS Data Management Center. Data from the TA network were made freely available as part of the EarthScope USArray facility, operated by Incorporated Research Institutions for Seismology (IRIS) and supported by the National Science Foundation, under Cooperative Agreements EAR-1261681. This work was supported by National Science Foundation grants EAR-1547594, EAR-0844187, and EAR-1727451. Constructive comments provided by Miaki Ishii and three anonymous reviewers helped improve the clarity of the manuscript.

Appendix A. Supplementary material

Supplementary material related to this article can be found online at https://doi.org/10.1016/j.epsl.2020.116214.

References

Armstrong, R.L., Taubeneck, W.H., Hales, P.O., 1977. Rb–Sr and K–Ar geochronometry of Mesozoic granitic rocks and their Sr isotopic composition, Oregon, Washington, and Idaho. Geol. Soc. Am. Bull. 88, 397–411. https://doi.org/10.1130/0016-7606(1977)88<397.

Brandon, A.D., Goles, G.G., 1988. A Miocene subcontinental plume in the Pacific Northwest: geochemical evidence. Earth Planet. Sci. Lett. 88, 273–283.

Cammarano, F., Goes, S., Vacher, P., Giardini, D., 2003. Inferring upper-mantle temperatures from seismic velocities. Phys. Earth Planet. Inter. 138, 197–222.

Camp, V.E., Hanan, B.B., 2008. A plume-triggered delamination origin for the Columbia River Basalt Group. Geosphere 4, 480–495. https://doi.org/10.1130/GES00175.1.

Camp, V.E., Ross, M.E., 2004. Mantle dynamics and genesis of mafic magmatism in the intermontane Pacific Northwest. J. Geophys. Res. 109, 1–14. https://doi.org/10.1029/2003JB002838.

Cox, C., Keller, G.R., Harder, S.H., 2013. A controlled-source seismic and gravity study of the high lava plains (HLP) of Eastern Oregon. Geochem. Geophys. Geosyst. 14, 5208–5226. https://doi.org/10.1002/2013GC004870.

Dahlen, F.A., Hung, S.-H., Nolet, G., 2000. Frechet kernels for finite-frequency traveltimes. I. Theory Geophys. J. Int. 141, 157–174.

Dalton, C.A., Bao, X., Ma, Z., 2017. The thermal structure of cratonic lithosphere from global Rayleigh wave attenuation. Earth Planet. Sci. Lett. 457, 250–262. https://doi.org/10.1016/j.epsl.2016.10.014.

Darold, A., Humphreys, E.D., 2013. Upper mantle seismic structure beneath the Pacific Northwest: a plume-triggered delamination origin for the Columbia River flood basalt eruptions. Earth Planet. Sci. Lett. 365, 232–242. https://doi.org/10.1016/j.epsl.2013.01.024.

Dasgupta, R., Mallik, A., Tsuno, K., Withers, A.C., Hirth, G., Hirschmann, M.M., 2013. Carbon-dioxide-rich silicate melt in the Earth's upper mantle. Nature 493, 211–226. https://doi.org/10.1038/nature11731.

Davenport, K.K., Hole, J.A., Tikoff, B., Russo, R.M., Harder, S.H., 2017. A strong contrast in crustal architecture from accreted terranes to craton, constrained by controlled source seismic data in Idaho and eastern Oregon. Lithosphere 9, 325–340. https://doi.org/10.1130/L553.1.

Draper, D.S., 1991. Late Cenozoic bimodal magmatism in the northern basin and range province of southeastern Oregon. J. Volcanol. Geotherm. Res. 47, 299–328. https://doi.org/10.1016/0377-0273(91)90006-L.

Duncan, R.A., 1982. A captured island chain in the Coast Range of Oregon and Washington. J. Geophys. Res. 87, 10827–10837.

Foster, D.A., Schafer, C., Fanning, C.M., Hyndman, D.W., 2001. Relationships between crustal partial melting, plutonism, orogeny, and exhumation: Idaho-Bitterroot batholith. Tectonophysics 342, 313–350.

Gao, H., 2015. Crustal seismic structure beneath the source area of the Columbia River flood basalt: bifurcation of the Moho driven by lithosphere delamination. Geophys. Res. Lett. 42, 9764–9771. https://doi.org/10.1002/2015GL066625.

Gaschnig, R.M., Vervoort, J.D., Lewis, R.S., Tikoff, B., 2011. Isotopic evolution of the Idaho Batholith and Challis Intrusive Province, Northern US Cordillera. J. Petrol. 12, 2397–2429. https://doi.org/10.1093/petrology/egr050.

Geist, D., Richards, M., 1993. Origin of the Columbia Plateau and Snake River Plain: deflection of the Yellowstone plume. Geology 21, 789–792. https://doi.org/10.1130/0091-7613(1993)021<0789:OOTC-PA>2.3.CO;2.

Goes, S., Govers, R., Vacher, P., 2000. Shallow mantle temperatures under Europe from P and S wave tomography. J. Geophys. Res. 105, 11,153–11,170.

Hales, T.C., Abt, D.L., Humphreys, E.D., Roering, J.J., 2005. Delamination origin for the Columbia River flood basalts and Wallowa Mountain uplift in NE Oregon, USA. Nature 438, 842–845. https://doi.org/10.1038/nature04313.

Hales, A.L., Doyle, H.A., 1967. P and S travel-time anomalies and their interpretation. Geophys. J. R. Astron. Soc. 13, 403–415.

Hamilton, W.B., 1989. Crustal geologic processes of the United States. In: Pakiser, L.C., Mooney, W.D. (Eds.), Geophysical Framework of the Continental United States. In: Geological Society of America Memoir, vol. 172, pp. 743–781.

Hammond, W.C., Humphreys, E.D., 2000. Upper mantle seismic wave attenuation: effects of realistic partial melt distribution. J. Geophys. Res. 105, 10987–10999.

Hammond, W.C., Toomey, D.R., 2003. Seismic velocity anisotropy and heterogeneity beneath the Mantle Electromagnetic and Tomography Experiment (MELT) region of the East Pacific Rise from analysis of P and S body waves. J. Geophys. Res. 108 (B4), 2176. https://doi.org/10.1029/2002JB001789.

Hawley, W.B., Allen, R.M., 2019. The fragmented death of the Farallon plate. Geophys. Res. Lett. 46, 7386–7394. https://doi.org/10.1029/2019GL083437.

Hooper, P.R., Binger, G.B., Lees, K.R., 2002. Ages of the Steens and Columbia River flood basalts and their relationship to extension-related calc-alkaline volcanism in eastern Oregon. Geol. Soc. Am. Bull. 114, 43–50. https://doi.org/10.1130/00167606(2002)114<0043:AOTSAC>2.0.CO;2.

Humphreys, E.D., Dueker, K.G., 1994. Western U.S. upper mantle structure. J. Geophys. Res. 99, 9615–9634.

Jarboe, N.A., Coe, R.S., Renne, P.R., Glen, J.M.G., 2010. The age of the Steens reversal and the Columbia River Basalt Group. Chem. Geol. 274, 158–168.

Karato, S., 1993. Importance of anelasticity in the interpretation of seismic tomography. Geophys. Res. Lett. 20, 1623–1626.

Kasbohm, J., Schoene, B., 2018. Rapid eruption of the Columbia River flood basalt and correlation with the mid-Miocene climate optimum. Sci. Adv., Geol. 4, eaat8223.

Kennett, B.L.N., Engdahl, E.R., 1991. Traveltimes for global earthquake location and phase identification. Geophys. J. Int. 105, 429–465.

Kincaid, C., Druken, K.A., Griffiths, R.W., Stegman, D.R., 2013. Bifurcation of the Yellowstone plume driven by subduction-induced mantle flow. Nat. Geosci. 6, 395–399. https://doi.org/10.1038/NGEO1774.

Knopoff, L., 1971. Attenuation. In: Coulomb, J., Caputo, M. (Eds.), Mantle and Core in Planetary Physics. Elsevier, New York, pp. 146–156.

Lee, C.-T.A., 2003. Compositional variation of density and seismic velocities in natural peridotites at STP conditions: implications for seismic imaging of compositional heterogeneities in the upper mantle. J. Geophys. Res. 108 (B9), 2441. https://doi.org/10.1029/2003JB002413.

Lerch, D.W., Klemperer, S.L., Glen, J.M.G., Ponce, D.A., Miller, E.L., Colgan, J.P., 2007. Crustal structure of the northwestern Basin and Range Province and its transition to unextended volcanic plateaus. Geochem. Geophys. Geosyst. 8, Q02011. https://doi.org/10.1029/2006GC001429.

Livaccari, R.F., 1991. Role of crustal thickening and extensional collapse in the tectonic evolution of the Sevier-Laramide orogeny, western United States. Geology 19, 1104–1107.

Manduca, C.A., Kuntz, M.A., Silver, L.T., 1993. Emplacement and deformation history of the western margin of the Idaho batholith near McCall, Idaho: influence of a major terrane boundary. Geol. Soc. Am. Bull. 105, 749–765. https://doi.org/10.1130/0016-7606(1993)105<0749:EADHOT>2.3.CO;2.

Mueller, P.A., Wooden, J.L., Mogk, D.W., Foster, D.A., 2011. Paleoproterozoic evolution of the Farmington zone: implications for terrane accretion in southwestern Laurentia. Lithosphere 3, 401–408. https://doi.org/10.1130/L161.1.

Paige, C.C., Saunders, M.A., 1982. LSQR: an algorithm for sparse linear equations and sparse least squares. ACM Trans. Math. Softw. 8, 43–71.

Reidel, S.P., Camp, V.E., Tolan, T.L., Martin, B.S., 2013. The Columbia River flood basalt province: stratigraphy, areal extent, volume, and physical volcanology. In: Reidel, S.P., Camp, V.E., Ross, M.E., Wolff, J.A., Martin, B.S., Tolan, T.L., Wells, R.E. (Eds.), The Columbia River Flood Basalt Province. Geological Society of America Special Paper 497.

Schmandt, B., Humphreys, E.D., 2010a. Seismic heterogeneity and small-scale convection in the southern California upper mantle. Geochem. Geophys. Geosyst. 11, Q05004. https://doi.org/10.1029/2010GC003042.

Schmandt, B., Humphreys, E.D., 2010b. Complex subduction and small-scale convection revealed by body-wave tomography of the western United States upper mantle. Earth Planet. Sci. Lett. 297, 435–445. https://doi.org/10.1016/j.epsl.2010.06.047.

Schmandt, B., Humphreys, E.D., 2011. Seismically imaged relict slab from the 55 ma Siletzia accretion to the northwest United States. Geology 39, 175–178. https://doi.org/10.1130/G31558.1.

Schutt, D.L., Lesher, C.E., 2006. Effects of melt depletion on the density and seismic velocity of garnet and spinel lherzolite. J. Geophys. Res. 111, B05401. https://doi.org/10.1029/2003JB002950.

Shen, W., Ritzwoller, M.H., 2016. Crustal and uppermost mantle structure beneath the United States. J. Geophys. Res., Solid Earth 121, 4306–4342. https://doi.org/10.1002/2016JB012887.

Shen, W., Ritzwoller, M.H., Schulte-Pelkum, V., 2013. A 3-D model of the crust and uppermost mantle beneath the central and western US by joint inversion of receiver functions and surface wave dispersion. Journal of Geophysical Research Solid Earth 118, 262–276. https://doi.org/10.1029/2012JB009602.

Smith, R.B., Jordan, M., Steinberger, B., Puskas, C.M., Farrell, J., Waite, J.P., Husen, S., Chang, W-L., O'Connell, R., 2009. Geodynamics of the Yellowstone hotspot and mantle plume: seismic and GPS imaging, kinematics, and mantle flow. J. Volcanol. Geotherm. Res. 188, 26–56. https://doi.org/10.1016/j.jvolgeores.2009.08.020.

Stanciu, A.C., Russo, R.M., Mocanu, V.I., Bremner, P.M., Hongsresawat, S., Torpey, M.E., VanDecar, J.C., Foster, D.A., Hole, J.A., 2016. Crustal structure beneath the Blue Mountains terranes and cratonic North America, eastern Oregon, and Idaho, from teleseismic receiver functions. J. Geophys. Res., Solid Earth 121, 5049–5067. https://doi.org/10.1002/2016JB012989.

VanDecar, J.C., Crosson, R.S., 1990. Determination of teleseismic relative phase arrival times using multi-channel cross-correlation and least squares. Bull. Seismol. Soc. Am. 80, 150–169.

Villagómez, D., Toomey, D.R., Geist, D.J., Hooft, E.E.E., Solomon, S.C., 2014. Mantle flow and multistage melting beneath the Galapagos hotspot revealed by seismic imaging. Nat. Geosci. 7, 151–156. https://doi.org/10.1038/ngeo2062.

Wells, R.E., Bukry, D., Friedman, R., Pyle, D., Duncan, R., Haeussler, P., Wooden, J., 2014. Geologic history of Siletzia, a large igneous province in the Oregon and Washington Coast Range: correlation to the geomagnetic polarity time scale and implications for a long-lived Yellowstone hotspot. Geosphere 10, 692–719. https://doi.org/10.1130/GES01018.1.

Wolff, J.A., Ramos, F.C., 2013. Source materials for the main phase of the Columbia River Basalt Group: geochemical evidence and implications for magma storage and transport. In: Reidel, S.P., Camp, V.E., Ross, M.E., Wolff, J.A., Martin,

B.S., Tolan, T.L., Wells, R.E. (Eds.), The Columbia River Flood Basalt Province, pp. 273–291. Geol. Soc. Am. Special Paper 497.

Wolff, J.A., Ramos, F.C., Hart, G.L., Patterson, J.D., Brandon, A.D., 2008. Columbia River flood basalts from a centralized crustal magmatic system. Nature Geoscience 1, 177–180. https://doi.org/10.1038/ngeo124.

Wolff, J.A., Steiner, A.R., Ramos, F.C., 2019. Origin of the Columbia River Flood Basalts: Geochemical Evidence, abstract presented at 2019 Annual Meeting. SSA, Seattle, Washington, 23–26 Apr.